

Machine Learning tools for global PDF fits

Juan Rojo*

*Department of Physics and Astronomy, VU University, De Boelelaan 1081, 1081 HV Amsterdam,
and Nikhef Theory Group, Science Park 105, 1098 XG Amsterdam, The Netherlands.*

E-mail: j.rojo@vu.nl

The use of machine learning algorithms in theoretical and experimental high-energy physics has experienced an impressive progress in recent years, with applications from trigger selection to jet substructure classification and detector simulation among many others. In this contribution, we review the machine learning tools used in the NNPDF family of global QCD analyses. These include multi-layer feed-forward neural networks for the model-independent parametrisation of parton distributions and fragmentation functions, genetic and covariance matrix adaptation algorithms for training and optimisation, and closure testing for the systematic validation of the fitting methodology.

*XXIIIth Quark Confinement and the Hadron Spectrum
1-6 August 2018
University of Maynooth, Ireland*

*Speaker.

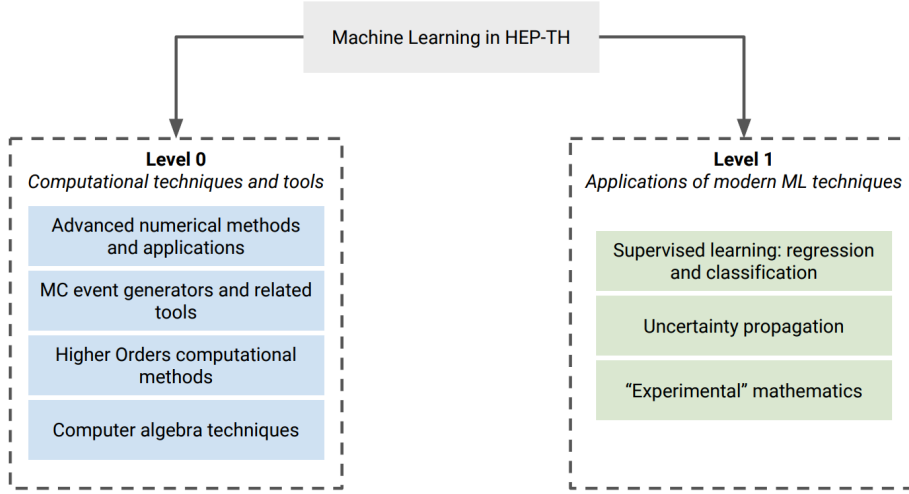


Figure 1: Machine learning tools in theoretical high-energy physics can be divided into two main categories: (i) computational techniques and tools, and (ii) applications of modern ML methods. Figure taken from [7].

Machine learning and high energy physics. The recent years have experienced an unprecedented boost in the quantity and quality of the applications of machine learning (ML) algorithms in both theoretical and experimental high-energy physics, as summarised in the recent Community White Paper [1] and in the review [2]. Similar developments have taken place in related areas such as astroparticle physics, the intensity frontier, and cosmology. In the context of LHC physics, machine learning tools have been exploited in applications ranging from detector simulation [3] to the exploration of the parameter space of New Physics scenarios [4] and the study of the substructure of hadronic jets [5], among several others. ML tools are even used in formal theory studies, for instance to explore the huge number of possible solutions (the landscape) predicted by string theory [6].

In the specific case of theoretical high-energy physics, a possible classification of the ML algorithms used was proposed in [7]. In the first category, one finds computational techniques and tools relevant for advanced numerical methods, Monte Carlo event generators, and higher-order perturbative calculations and computer algebra among others. The second category includes applications of modern ML techniques such as supervised learning (regression and classification), uncertainty propagation, and even “experimental” mathematics.

In the context of LHC phenomenology, an important ingredient of theoretical predictions for event rates are the parton distribution functions (PDFs) of the proton [8], describing the momentum distribution that quarks and gluons (as well as photons [9]) carry in the initial stage of the hadronic collision. These PDFs are determined from non-perturbative dynamics, and therefore their computation from first principles is extremely challenging (see however encouraging progress from lattice QCD [10]). Therefore, they need to be extracted from experimental data by means of the so-called global QCD analysis. As discussed in this contribution, also for this specific application machine learning tools have shown to be highly effective, from the use of artificial neural networks as universal unbiased interpolants to advanced optimisation strategies for the exploration of complex high-dimensional parameter spaces.

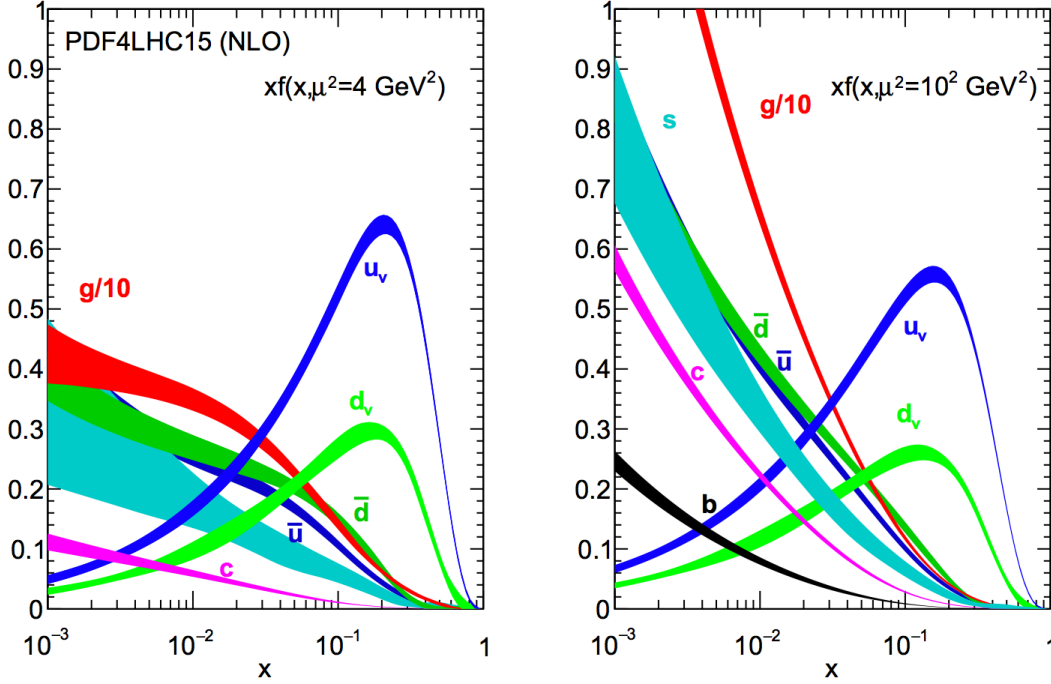


Figure 2: The parton distributions from the PDF4LHC15 NLO set for a low scale, $Q = 2$ GeV, where the PDFs are parametrised, and a higher scale $Q = 10$ GeV, highlighting the impact of DGLAP evolution.

In a nutshell, the main task of the global QCD analysis is to determine the parton distributions of the proton at some low scale Q_0 , and then evolve them upwards to higher energies to carry out predictions for LHC processes, say for Higgs production. In Fig. 2 we show the NLO PDF4LHC15 set [11, 12] both at $Q = 2$ GeV, close to the typical scale where the PDFs are parametrised, and at a higher scale $Q = 10$ GeV, highlighting the effects of DGLAP evolution. We can observe how for $x \lesssim 0.01$ the perturbative QCD evolution drives a steep rise in the gluon and the sea quarks.

Machine learning tools in the NNPDF framework. The NNPDF approach to global QCD analyses has been successfully applied to the determination of the unpolarised [13] and polarised [14] parton distributions of the proton as well as to the light-hadron identified and the unidentified fragmentation functions (FFs) [15, 16]. The latter are the time-like counterparts of the PDFs, and describe the hadronisation process of colored partons into color neutral-hadrons. There is also work in progress towards NNPDF fits of nuclear modification factors, relevant for the interpretation of heavy-ion collisions at RHIC and the LHC.

In Fig. 3 we indicate the different components that constitute the NNPDF family of global analyses, highlighting those that involve machine learning algorithms. As illustrated there, a global QCD fit is based on three main inputs: experimental data, higher-order perturbative calculations in both QCD and QED/electroweak theory, and a statistical framework dealing with aspects such as the PDF parametrisation and their uncertainty estimate and propagation.

These three ingredients are combined in the global QCD fit by means of the minimisation of a suitably defined figure of merit, the χ^2 , which includes all relevant sources of uncertainty and which leads to the determination of the parameters that define the PDF shape. Experimental

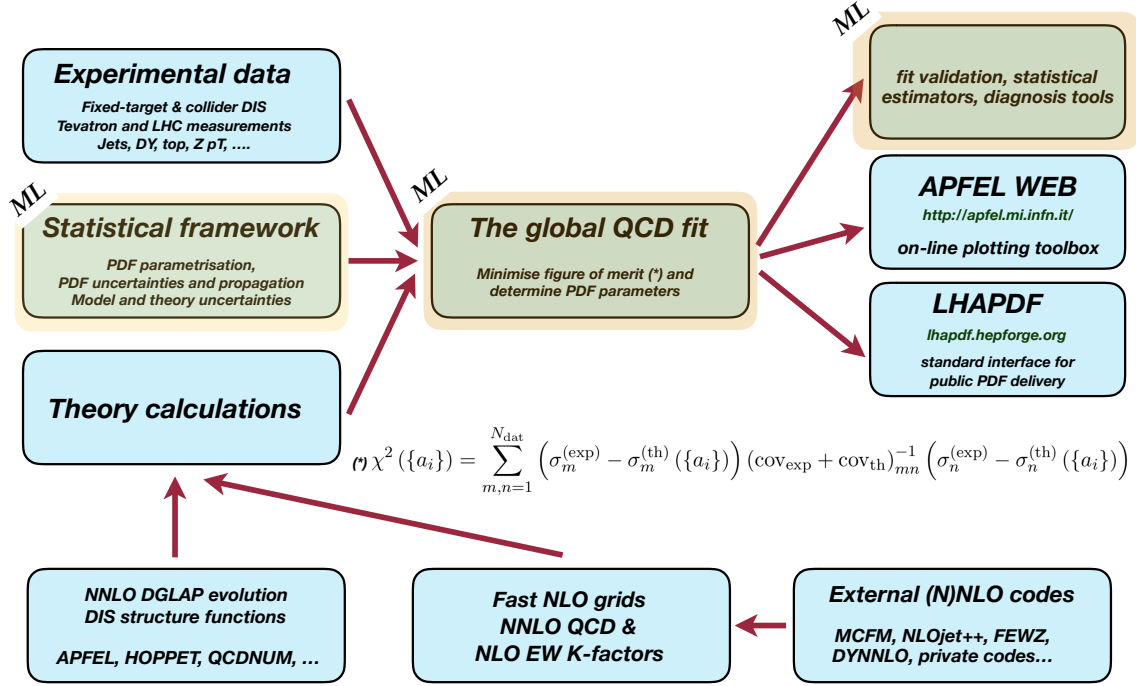


Figure 3: Representation of the different components that constitute the NNPDF family of global QCD analysis, highlighting those that exploit machine learning tools.

uncertainties are propagated to the PDFs by means of the Monte Carlo replica method, which allows constructing a representation of the probability density in the space of PDFs. Afterwards, the fit is validated using a range of complementary diagnosis tools and it can be plotted in different ways. Finally, the PDF fit is translated into the LHAPDF standard interface, suitable for its public delivery and its integration into other HEP codes and into the analysis framework of the LHC experiments.

As shown in Fig. 3, machine learning tools arise in various components of the NNPDF framework, including the strategy for the PDF parametrisation, the optimisation (training) that defines the best-fit parameters, and the subsequent validation by means of closure testing. We describe now each of these aspects in turn.

PDF parametrisation and neural networks. In the NNPDF approach, the parton distribution functions (or the fragmentation functions) are parameterized at a low scale, around the boundary between the perturbative and non-perturbative regimes of QCD, namely $Q_0 \simeq 1$ GeV (the proton mass). As opposed to other fitting approaches, where the PDF shape is parametrised in terms of relatively simple functional forms more or less inspired in QCD models (see [17] for an overview), we use artificial neural networks (NNs) as unbiased interpolants. This allows us to avoid the theoretical biases that can be incurred when specific model functional forms are adopted. Note here that QCD provides only very limited guidance about the behaviour of PDFs at the input parametrisation scale Q_0 , such as integrability conditions and the momentum and valence sum rules, and does not provide any further information on their x dependence at low scales.

Specifically, in the NNPDF fits we use multi-layer feed-forward artificial neural networks

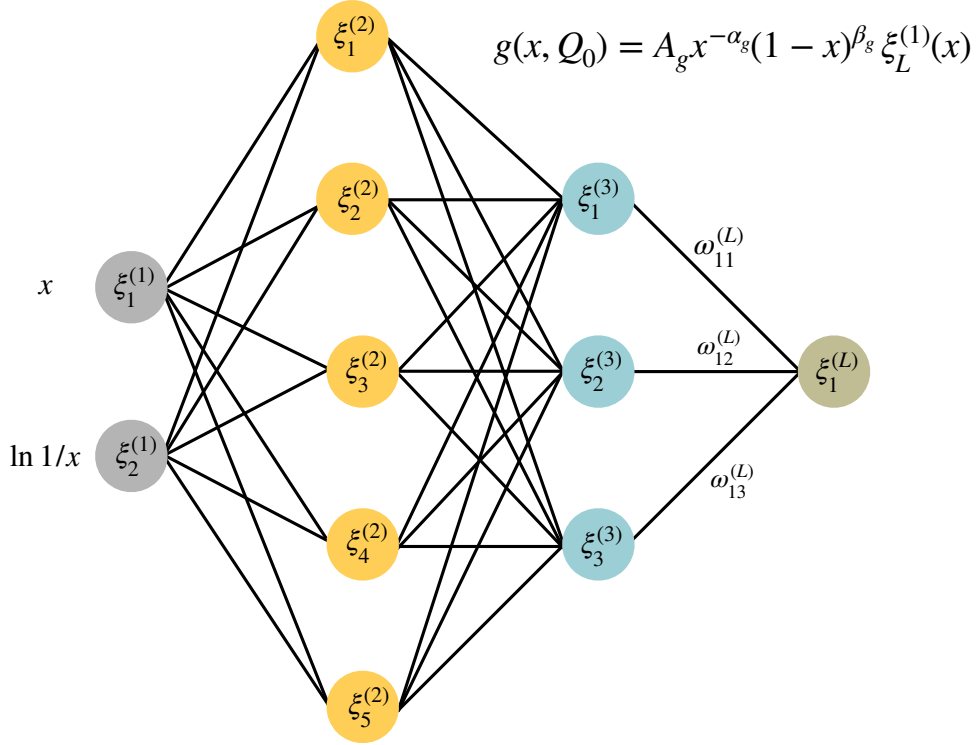


Figure 4: A multi-layer feed-forward artificial neural network (perceptron) such as the one used in the NNPDF global analysis. This specific network has a 2-5-3-1 architecture with two inputs (x and $\ln 1/x$) and one output neuron, which is directly related to the value of the PDF at the input parametrisation scale Q_0 , as indicated by Eq. (1).

(perceptrons) such as the one shown in Fig. 4. This NN has a 2-5-3-1 architecture with two inputs (x and $\ln 1/x$) and one output neuron, which is directly related to the value of the PDF at the input parametrisation scale Q_0 . The activation state of each neuron is denoted by $\xi_i^{(l)}$, with l labelling the layer and i the specific neuron within each layer. The values of the activation states of the neurons in layer l are evaluated in terms of those of the previous layer ($l-1$) and the weights $\{\omega_{ij}^{(l)}\}$ connecting them as well as by the activation thresholds of each neuron $\{\theta_i^{(l)}\}$, see [18] and references therein. The training of the NN in this context corresponds to determining the values of the weights and thresholds that fulfill the constraints of a given optimisation problem as discussed below.

The value of a given PDF, say the gluon, at the input parametrisation scale Q_0 is then given in terms of the activation state of the neuron in the last layer as follows

$$g(x, Q_0) = A_g x^{-\alpha_g} (1-x)^{\beta_g} \xi_1^{(L)}(x), \quad (1)$$

where A_g is here an overall normalisation constant fixed by the momentum sum rule. The $x^{-\alpha_g} (1-x)^{\beta_g}$ term is known as the preprocessing factor and facilitates the NN training by allowing to learn a smoother function without introducing any bias in the fits. The values of the exponents $\{\alpha, \beta\}$ are chosen at random in an interval determined iteratively [19].

The use of NNs as universal unbiased interpolants offers a number of important advantages in the context of the global PDF fit. In particular, they ensure that the fit results are driven only by

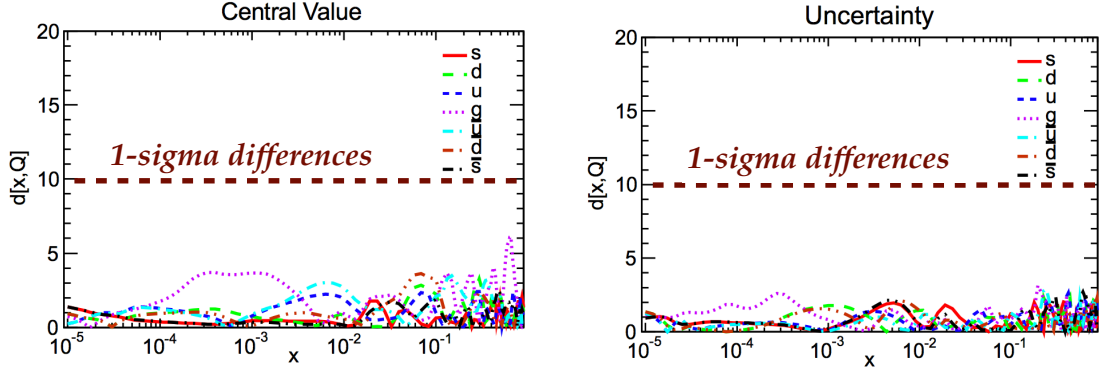


Figure 5: The statistical distances between the seven PDFs (for both central values and uncertainties) in NNPDF3.0 fits using either the 2-5-3-1 or the 2-20-5-1 architecture. The dotted line indicates the one-sigma difference for the case of $N_{\text{rep}} = 100$ replicas relevant here.

the input data and theory, but not by model-dependent assumptions. Specifically, we have shown that the NNPDF fits are stable with respect to changes in the quark flavour basis, the value of the input scale Q_0 , and the NN architecture (provided we work in the redundant regime). In the latter case, we have verified that even increasing the number of fitted parameters by an order of magnitude (from around 400 parameters with 2-5-3-1 to around 4000 parameters with the 2-20-5-1 architecture) leads to results at the PDF level which are statistically equivalent [19].

This last property is illustrated in Fig. 5, where we show the statistical distances [20] between the seven fitted PDFs, for both central values and uncertainties, in NNPDF3.0 fits using either the 2-5-3-1 or the 2-20-5-1 architectures. The dotted line indicates the value of one-sigma differences for the case of $N_{\text{rep}} = 100$ replicas, relevant in this comparison. We thus find that the effect of increasing the number of fitted parameters by an order of magnitude is much smaller than the PDF uncertainties themselves.

Optimisation and training algorithms. The training (also known as learning or optimisation phase) of neural networks is carried out in most cases using some variant of the gradient descent method, such as back-propagation [21] or stochastic gradient descent. In these methods, the determination of the fit parameters (namely the weights and thresholds of the NN) requires the evaluation of the gradients of χ^2 , that is,

$$\frac{\partial \chi^2}{\partial w_{ij}^{(l)}}, \quad \frac{\partial \chi^2}{\partial \theta_i^{(l)}}. \quad (2)$$

Computing these gradients in the NNPDF case would be quite involved due to the non-linear relation between the fitted experimental data and the input PDFs, which proceeds through convolutions both with the DGLAP evolution kernels and the hard-scattering partonic cross-sections as encoded into the optimised APFELgrid fast interpolation strategy [22, 23].

The theory prediction for a collider cross-section in terms of the NN parameters reads

$$\sigma^{(\text{th})}(\{\omega, \theta\}) = \hat{\sigma}_{ij}(Q^2) \otimes \Gamma_{ij,kl}(Q^2, Q_0^2) \otimes q_k(Q_0, \{\omega, \theta\}) \otimes q_l(Q_0, \{\omega, \theta\}) \quad (3)$$

where \otimes indicates a convolution over x , $\hat{\sigma}_{ij}$ and $\Gamma_{ij,kl}$ stand for the hard-scattering cross-sections and the DGLAP evolution kernels respectively, and sum over repeated flavour indices is under-

stood. In the APFELgrid approach, this cross-section can be expressed in a much compact way as

$$\sigma^{(\text{th})}(\{\omega, \theta\}) = \sum_{i,j=1}^{n_f} \sum_{a,b=1}^{n_x} \text{FK}_{k,ij,ab} \cdot q_i(x_a, Q_0, \{\omega, \theta\}) \cdot q_j(x_b, Q_0, \{\omega, \theta\}), \quad (4)$$

where now all perturbative information is pre-computed and stored in the $\text{FK}_{k,ij,ab}$ interpolation tables, and a, b run over a grid in x . The convoluted relation between $\sigma^{(\text{th})}$ and the NN parameters in Eq. (4) is what makes the implementation of gradient descent methods challenging.

In the proton NNPDF global analysis, both in the polarised and the unpolarised case, the NN training is carried out instead by means Genetic Algorithms (GAs). GAs [24] are based on a combination of deterministic and stochastic ingredients which make them particularly useful to explore complex parameter spaced without getting stuck in local minima, and which do not require the knowledge of the χ^2 gradients in Eq. (2) but only of its local values.

As illustrated in Fig. 6, at each iteration of the fit, variations of the PDF parameters denoted as PDFs are generated by random adjustment of the previous best-fit neural-network parameters. The mutant PDF parameters with the lowest values of the figure of merit χ^2 quantifying the agreement with data are then selected as the best-fit for the next iteration. Clearly, such procedure is not sensitive to the higher-order structure of the problem in the parameter space, and thus while being more flexible and requiring only local χ^2 values, it is bound to be less efficient than gradient descent. In the NNPDF3 family of global analysis, an optimised GA has been adopted with parameters tuned by means of the closure tests discussed below.

Alternative optimisation strategies have been explored within our Collaboration. One important example is the Covariance Matrix Adaption - Evolutionary Strategy (CMA-ES) family of algorithms [25, 26], used in the NNPDF determinations of fragmentation functions. Here we briefly summarize the main features of this training algorithm. We denote the set of fit parameters $\{\omega_{ij}^{(i)}, \theta_i^{(i)}\}$ (weights and thresholds of the NNs) as a single vector $\mathbf{a}^{(i)}$. In the following, the superscript i indicates the values at the i^{th} iteration. The fit parameters are initialised at the beginning of the fit according to a multi-Gaussian distribution \mathcal{N} with zero mean and unit covariance

$$\mathbf{a}^{(0)} \sim \mathcal{N}(0, \mathbf{C}^{(0)}), \quad \mathbf{C}^{(0)} = \mathbf{I}. \quad (5)$$

where we use \sim to denote the distribution of the random vector. This vector is used as the centre of a search distribution in the fitting parameter space. At every iteration of the algorithm, λ mutants $\mathbf{x}_1, \dots, \mathbf{x}_\lambda$ of the NN parameters are generated by means of the following rule:

$$\mathbf{x}_k^{(i)} \sim \mathbf{a}^{(i-1)} + \sigma^{(i-1)} \mathcal{N}(0, \mathbf{C}^{(i-1)}), \quad k = 1, \dots, \lambda, \quad (6)$$

in other words, mutants are generated around the search centre according to a multi-Gaussian \mathcal{N} with covariance $\mathbf{C}^{(i)}$ and according to a step-size $\sigma^{(i)}$. The mutants are then sorted according to their value of the figure of merit such that $\chi^2(\mathbf{x}_k) < \chi^2(\mathbf{x}_{k+1})$. Subsequently, the new search centre is computed as a weighted average over a fixed fraction of the best mutants

$$\mathbf{a}^{(i)} = \mathbf{a}^{(i-1)} + \sum_{k=1}^{\mu=\lambda/2} w_k \left(\mathbf{x}_k^{(i)} - \mathbf{a}^{(i-1)} \right), \quad (7)$$

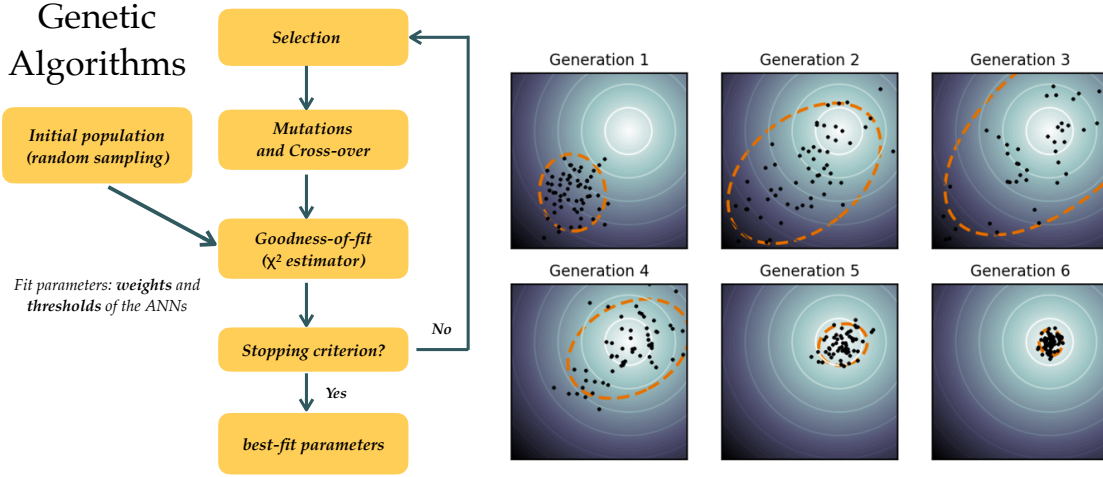


Figure 6: Left: Genetic Algorithms work by means of an efficient combination of deterministic and stochastic ingredients. Right: schematic representation of how the CMA-ES algorithm works in a toy scenario, showing how it manages to approach the global minimum while at the same time stochastically sampling the region around it.

where the $\{W_k\}$ are parameters of the CMA-ES algorithm which have been independently tuned for similar applications.

The most important feature of the CMA-ES algorithms is that both the step size $\sigma^{(i)}$ and the search distribution covariance matrix $\mathbf{C}^{(i)}$ are being optimised by the fit procedure. To achieve this, the information present in the ensemble of mutants is used to learn preferred directions in parameter space without the need for the explicit computation of the gradients of the χ^2 . This adaptive behaviour improves the efficiency of the minimisation procedure in comparison to the traditional genetic algorithm described above. Note also that each iteration's best fit is computed from the weighted average over a subset of mutants, rather than taking only the mutant with smaller value of the χ^2 . In this way, the effects of the possible statistical fluctuations in the χ^2 are reduced.

In Fig. 6 we display an schematic representation of how the CMA-ES algorithm works in a toy scenario, showing how it manages to approach the global minimum while at the same time stochastically sampling the region around it. Starting from a random population of solutions far from the minimum (white region), the spread (variance) of the population increases while at the same time the average (center) solution moves closer to the minimum. As the number of generations increases, the average solution remains close to the minimum but now the variance has been reduced significantly, indicating that the algorithm has converged.

As mentioned above, a common feature of both GA and CMA-ES is that they do not require knowledge (analytical or numerical) of the gradients of the χ^2 function in the fitting parameter space. There is now ongoing work within the Collaboration towards the analytical evaluation of these gradients in terms of the NN parameters and the perturbative information encoded in Eq. (4), which would make possible adopting efficient optimisation techniques such as stochastic gradient descent and back-propagation. If successful, the program of adopting gradient-based methods should lead to a significant speed-up of the NNPDF fits, which in the proton case now take between one and three days per Monte Carlo replica, depending on the processor details.

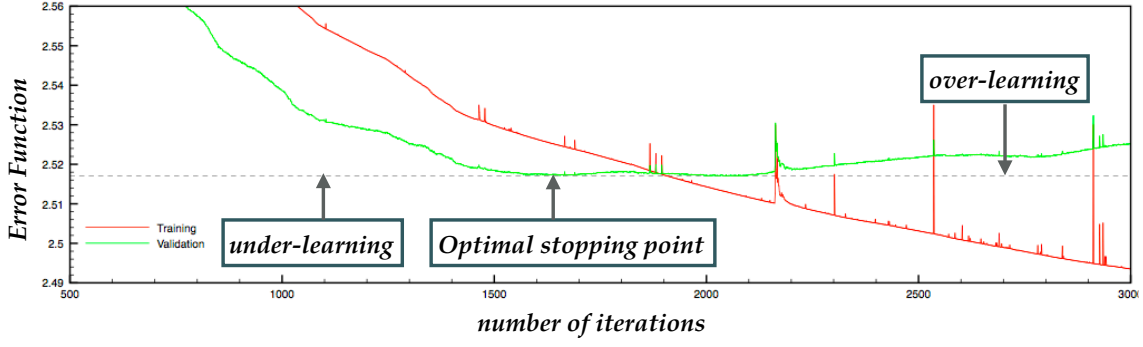


Figure 7: Schematic representation of the look-back cross-validation stopping used in the NNPDF fits.

The use of a highly redundant parametrisation such as that illustrated in Fig. 4 raises the worry that one might end up fitting point-to-point fluctuations. In order to avoid this situation, known as overfitting (learning the statistical fluctuations of the input experimental data rather than the underlying experimental data), a suitable regularisation strategy must be adopted. In the NNPDF fits, we use the look-back cross-validation stopping criterion, described in [19], and illustrated schematically in Fig. 7.

This cross-validation stopping strategy works as follows. First of all, the input experimental measurements are divided into two categories at random, the training sample and the validation sample, typically with equal probability. Only the former is used in the fit, while the latter plays the role of a control sample used to monitor and validate the training progress. The optimal stopping point is defined as the global minimum of the χ^2 of the validation sample, computed over a large fixed number of iterations (hence the name “look-back”). As shown in Fig. 7, a shorter fit would result in under-learning (where the NN has not properly learned yet the underlying law) while a longer fit instead leads to over-learning (where the NN ends up fitting statistical fluctuations). The tell-tale sign of the latter is the increase of the validation χ^2 increases (rather than the decrease) as the number of iterations increases, indicating that what is being learned in the training sample is not present in the validation one (namely the fluctuations).

Closure testing. Fitting experimental data is often complicated by a number of factors unrelated to the methodology itself, such as possible dataset inconsistencies (either internal or external) or inadequacies of the theoretical description adopted. Therefore, it is far from optimal to assess the benefits of a specific fitting methodology by applying it to the actual data, while it is much more robust to test it instead in an analysis of pseudo-data generated from a fixed (known) underlying theory.

In these so-called closure tests, one assumes that PDFs at the input scale Q_0 correspond to a specific model (say MMHT14 or CT14), generate pseudo-data accordingly, and then carry out the NNPDF global fit. Since in this case the “true result” of the fit is known by construction, it is possible to systematically validate the results verifying for example that central values are reproduced and fluctuate as indicated by the PDF uncertainties, or that the χ^2 values obtained are those that correspond to the generated pseudo-data. Additionally, one can verify that PDF reweighting based on Bayesian inference [27, 28] reproduces the fit results, providing a further

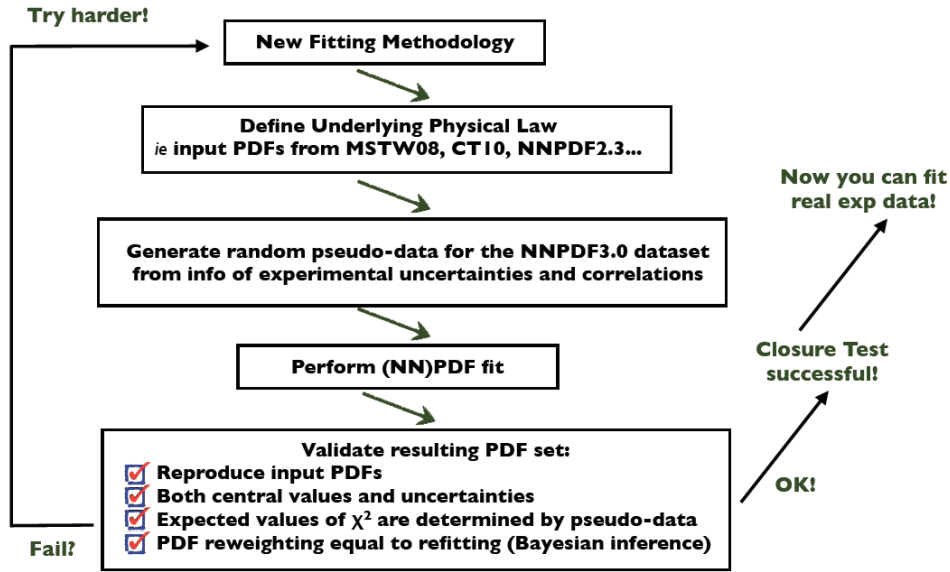


Figure 8: Flow-chart indicating how a given PDF fitting methodology can be closure tested in order to demonstrate the statistical robustness of its results.

cross-check that the resulting PDF uncertainties admit a robust statistical interpretation. In Fig. 8 we show a flow chart indicating how a given fitted methodology can be closure tested in order to demonstrate the statistical robustness of its results.

In Fig. 9 we display some representative results of the closure testing of the NNPDF3.0 fits. Closure tests can be performed at Level 0, 1, or 2, depending on the amount of fluctuation added on top of the generated pseudo-data. In particular, in Level 0 closure tests no fluctuations are added, while Level 2 corresponds to the same amount of fluctuations as in the real global fits (Level 1 is the intermediate case). First of all, in the left plot we show how at Level 0 the χ^2 becomes arbitrarily small since there exist at least one solution (the input PDF set) that corresponds to $\chi^2 = 0$. We also show the improved performance of the NNPDF3.0 GAs as compared to the previous one used in the NNPDF2.3 fit. Secondly, in the right plot we display the distribution of single replica fits in a Level 2 closure test, showing that central values fluctuate in accordance with the quoted PDF uncertainties as they should (indicated by the good agreement with a Gaussian distribution). Several other estimators can be studied to further validate the results of these closure test exercises.

Acknowledgments. We are grateful to T. Dorigo and S. Gleyzer for their invitation to given this talk at QCHS13. This work has been supported by the ERC Starting Grant “PDF4BSM” and by the Netherlands Organisation for Scientific Research (NWO).

References

- [1] K. Albertsson et al., *Machine Learning in High Energy Physics Community White Paper*, [arXiv:1807.02876](https://arxiv.org/abs/1807.02876).
- [2] A. Radovic, M. Williams, D. Rousseau, M. Kagan, D. Bonacorsi, A. Himmel, A. Aurisano, K. Terao,

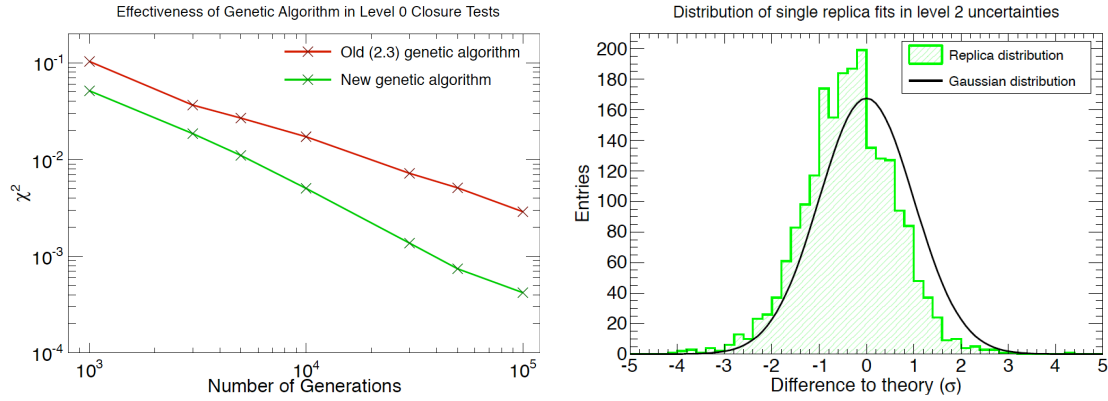


Figure 9: Representative results of the closure testing of the NNPDF3.0 fits. Left: at Level 0, the χ^2 becomes arbitrarily small since there exist at least one solution (the input PDF set) that corresponds to $\chi^2 = 0$. We also show the improved performance of the NNPDF3.0 GAs as compared to the previous one used in the NNPDF2.3 fit. Right: the distribution of single replica fits in a Level 2 closure test, showing that central values fluctuate in accordance with the quoted PDF uncertainties as they should.

and T. Wongjirad, *Machine learning at the energy and intensity frontiers of particle physics*, *Nature* **560** (2018), no. 7716 41–48.

- [3] M. Paganini, L. de Oliveira, and B. Nachman, *CaloGAN : Simulating 3D high energy particle showers in multilayer electromagnetic calorimeters with generative adversarial networks*, *Phys. Rev. D* **97** (2018), no. 1 014021, [[arXiv:1712.10321](#)].
- [4] S. Caron, J. S. Kim, K. Rolbiecki, R. Ruiz de Austri, and B. Stienen, *The BSM-AI project: SUSY-AI—generalizing LHC limits on supersymmetry with machine learning*, *Eur. Phys. J. C* **77** (2017), no. 4 257, [[arXiv:1605.02797](#)].
- [5] A. J. Larkoski, I. Moult, and B. Nachman, *Jet Substructure at the Large Hadron Collider: A Review of Recent Advances in Theory and Machine Learning*, [arXiv:1709.04464](#).
- [6] J. Carifio, J. Halverson, D. Krioukov, and B. D. Nelson, *Machine Learning in the String Landscape*, *JHEP* **09** (2017) 157, [[arXiv:1707.00655](#)].
- [7] S. Carrazza, *Machine learning challenges in theoretical HEP*, in *18th International Workshop on Advanced Computing and Analysis Techniques in Physics Research (ACAT 2017) Seattle, WA, USA, August 21-25, 2017*, 2017. [arXiv:1711.10840](#).
- [8] J. Gao, L. Harland-Lang, and J. Rojo, *The Structure of the Proton in the LHC Precision Era*, *Phys. Rept.* **742** (2018) 1–121, [[arXiv:1709.04922](#)].
- [9] NNPDF Collaboration, V. Bertone, S. Carrazza, N. P. Hartland, and J. Rojo, *Illuminating the photon content of the proton within a global PDF analysis*, *SciPost Phys.* **5** (2018) 008, [[arXiv:1712.07053](#)].
- [10] H.-W. Lin et al., *Parton distributions and lattice QCD calculations: a community white paper*, *Prog. Part. Nucl. Phys.* **100** (2018) 107–160, [[arXiv:1711.07916](#)].
- [11] J. Butterworth et al., *PDF4LHC recommendations for LHC Run II*, *J. Phys. G* **43** (2016) 023001, [[arXiv:1510.03865](#)].

- [12] S. Carrazza, J. I. Latorre, J. Rojo, and G. Watt, *A compression algorithm for the combination of PDF sets*, *Eur. Phys. J.* **C75** (2015) 474, [[arXiv:1504.06469](#)].
- [13] **NNPDF** Collaboration, R. D. Ball et al., *Parton distributions from high-precision collider data*, *Eur. Phys. J.* **C77** (2017), no. 10 663, [[arXiv:1706.00428](#)].
- [14] **NNPDF Collaboration** Collaboration, E. R. Nocera, R. D. Ball, S. Forte, G. Ridolfi, and J. Rojo, *A first unbiased global determination of polarized PDFs and their uncertainties*, *Nucl.Phys.* **B887** (2014) 276, [[arXiv:1406.5539](#)].
- [15] **NNPDF** Collaboration, V. Bertone, S. Carrazza, N. P. Hartland, E. R. Nocera, and J. Rojo, *A determination of the fragmentation functions of pions, kaons, and protons with faithful uncertainties*, *Eur. Phys. J.* **C77** (2017), no. 8 516, [[arXiv:1706.07049](#)].
- [16] **NNPDF** Collaboration, V. Bertone, N. P. Hartland, E. R. Nocera, J. Rojo, and L. Rottoli, *Charged hadron fragmentation functions from collider data*, *Eur. Phys. J.* **C78** (2018), no. 8 651, [[arXiv:1807.03310](#)].
- [17] R. D. Ball, E. R. Nocera, and J. Rojo, *The asymptotic behaviour of parton distributions at small and large x* , *Eur. Phys. J.* **C76** (2016), no. 7 383, [[arXiv:1604.00024](#)].
- [18] **The NNPDF** Collaboration, R. D. Ball et al., *A determination of parton distributions with faithful uncertainty estimation*, *Nucl. Phys.* **B809** (2009) 1–63, [[arXiv:0808.1231](#)].
- [19] **NNPDF** Collaboration, R. D. Ball et al., *Parton distributions for the LHC Run II*, *JHEP* **04** (2015) 040, [[arXiv:1410.8849](#)].
- [20] **The NNPDF** Collaboration, R. D. Ball et al., *A first unbiased global NLO determination of parton distributions and their uncertainties*, *Nucl. Phys.* **B838** (2010) 136, [[arXiv:1002.4407](#)].
- [21] S. Forte, L. Garrido, J. I. Latorre, and A. Piccione, *Neural network parametrization of deep-inelastic structure functions*, *JHEP* **05** (2002) 062, [[hep-ph/0204232](#)].
- [22] V. Bertone, S. Carrazza, and J. Rojo, *APFEL: A PDF Evolution Library with QED corrections*, *Comput.Phys.Commun.* **185** (2014) 1647–1668, [[arXiv:1310.1394](#)].
- [23] V. Bertone, S. Carrazza, and N. P. Hartland, *APFELgrid: a high performance tool for parton density determinations*, *Comput. Phys. Commun.* **212** (2017) 205–209, [[arXiv:1605.02070](#)].
- [24] J. Rojo and J. I. Latorre, *Neural network parametrization of spectral functions from hadronic tau decays and determination of qcd vacuum condensates*, *JHEP* **01** (2004) 055, [[hep-ph/0401047](#)].
- [25] N. Hansen, *The CMA Evolution Strategy: A Comparing Review*, pp. 75–102. Springer Berlin Heidelberg, Berlin, Heidelberg, 2006.
- [26] N. Hansen, *The CMA evolution strategy: A tutorial*, *CoRR* **abs/1604.00772** (2016).
- [27] **The NNPDF** Collaboration, R. D. Ball et al., *Reweighting NNPDFs: the W lepton asymmetry*, *Nucl. Phys.* **B849** (2011) 112–143, [[arXiv:1012.0836](#)].
- [28] R. D. Ball, V. Bertone, F. Cerutti, L. Del Debbio, S. Forte, et al., *Reweighting and Unweighting of Parton Distributions and the LHC W lepton asymmetry data*, *Nucl.Phys.* **B855** (2012) 608–638, [[arXiv:1108.1758](#)].